IOP Publishing

Plasma Sources Science and Technology

Plasma Sources Sci. Technol. **23** (2014) 065045 (10pp)

doi:10.1088/0963-0252/23/6/065045

Experimental investigation of a surface DBD plasma actuator at atmospheric pressure in different N_2/O_2 gas mixtures

P Audier[1,2], H Rabat[1], A Leroy[2] and D Hong[1]

[1] Univ. Orléans, CNRS, GREMI, UMR 7344, France
[2] Univ. Orléans, PRISME, INSA-CVL, France

E-mail: audier.pierre@gmail.com

Received 21 March 2014, revised 24 August 2014
Accepted for publication 5 September 2014
Published 4 November 2014

Abstract

This paper presents an investigation of the influence of nitrogen and oxygen on the behavior of a surface dielectric barrier discharge (SDBD) used for active flow control. The SDBD operated in a controlled atmosphere under several N_2/O_2 gas mixture ratios. For each gas mixture, the consumed power was measured as a function of voltage amplitude. Then, for a given applied high voltage, the plasma morphology was recorded and commented and lastly, ionic wind velocity measurements were performed. Results show that the induced ionic wind velocity is mainly due to oxygen negative ions during the negative half-cycle. Nevertheless, the contribution of nitrogen to velocity is not negligible during the positive half-cycle. Moreover, the propagation of negative spark filaments during the negative half-cycle is linked to the proportion of O_2 in the gas mixture. Increasing this proportion beyond 20% leads to a shift in the saturation effect to lower voltages and to a decrease in the maximum ionic wind velocity value.

Keywords: plasma, DBD, flow control, discharge, ionic wind, oxygen, nitrogen

(Some figures may appear in colour only in the online journal)

1. Introduction

Surface dielectric barrier discharges (SDBDs) are currently studied in aerodynamic research as actuators for active flow control around aerodynamic geometries. Over the last decade, flow control by plasma actuators has been extensively studied in order to manipulate external flows on aerodynamic geometries. Recent papers [1–3] give an overview of various configurations based on the SDBD and highlight the ability of this type of actuator to manipulate flows [4–7]. Typically, a surface plasma actuator operates by applying a high voltage, usually of sine waveform, between two electrodes separated by a dielectric material. Due to the strong electric field, a non-thermal plasma is created above the dielectric where a low density of electrons, positive and negative ions and neutral particles coexist. Interactions between air and plasma result in a wall tangential jet flow, called ionic wind, due to a self-sustaining process involving a high rate of collisions between neutral and charged particles [8, 9]. The SDBD evolves as a set of micro-discharges repeating each half-cycle of the applied high voltage sine waveform: streamer discharge during the positive-going half-cycle, characterized by high current pulses and glow discharge during the negative-going half-cycle characterized by small current pulses [2].

As one of the main goals of plasma actuators is to manipulate external flows, specially for aeronautical applications, a global investigation into the atmospheric effects on SDBD actuators operating in different pressure, humidity and temperature conditions was conducted. Few studies have been performed in real flight pressure and temperature conditions. Benard *et al* [10] observed that the maximum induced velocity increased when the ambient pressure decreased from 1 to 0.6 atm, but decreased for lower pressures, while Versailles *et al* [11] investigated the impact of temperature on the induced body force and observed an almost linear increase of this force with increasing temperature.

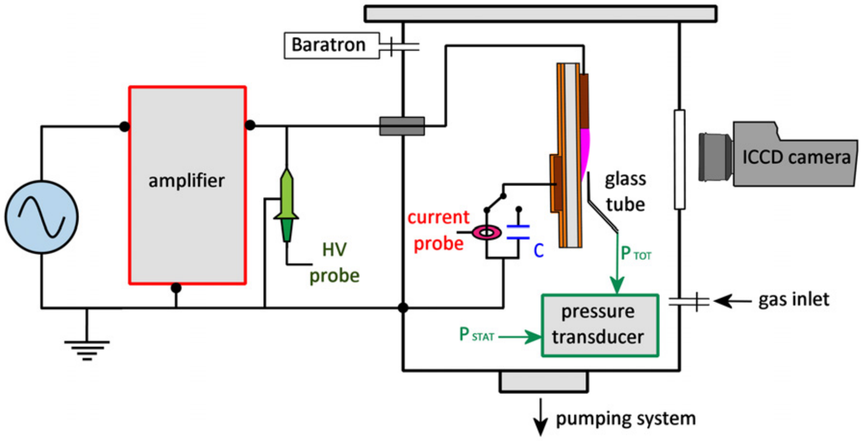

Figure 1. Experimental set-up for measurements of a SDBD operating in controlled atmosphere. To measure the dissipated power, a dipole capacitor was used due to the switch.

Anderson and Roy evaluated how the relative humidity rate affected SDBD performances [12] and demonstrated that the actuator can be used with a high humidity rate. ICCD imaging measurements conducted by Leonov *et al* [13] demonstrated that the morphology of plasma filaments is influenced by the gas composition. They observed that in nitrogen, a slow wave of near surface luminosity exists in contrast to a weak constant glow in air. Benard *et al* also observed, with ICCD imaging measurements, that while the pressure effect appeared to be dominant, a change in the filament propagation occurred depending on the altitude or the temperature [14].

Because of its complexity, the mechanism of the momentum transfer of ions and electrons with neutral gas molecules is currently under investigation, although several important results have already been published. Forte *et al* [15] used optical phase-resolved techniques to measure the time evolution of velocity and showed that the velocity value is higher during the negative-going half-cycle. Using phase-locked particle image velocimetry, Kim *et al* [16] showed that oxygen negative ions play a dominant role in plasma actuation. By using the actuator to drive a second-order mechanical system, Enloe *et al* [17] showed that the great majority (97%) of the momentum coupling occurs during the negative-going portion of the discharge cycle. Finally, Leonov *et al* [13] established the principal role of negative ions in plasma-induced flow generation during the negative-going half-cycle by using time-resolved pressure measurements in air and nitrogen at atmospheric pressure. The main contribution to momentum transfer during this half-cycle was also pointed out by Lagmich *et al* [8] and by Soloviev [18] using numerical simulation. The latter paper also discussed in detail a so-called saturation effect of the ionic wind. Indeed, at the beginning, the ionic wind velocity increases as the input power increases, but a change in plasma morphology occurs when the power input becomes too high. Forte *et al* [15] noticed that this saturation corresponds to a transition from a diffuse discharge regime to a filamentary one, where strong energetic filaments appear at the surface of the dielectric. Thomas *et al* [19] reported that the maximum body force produced by a SDBD plasma actuator is limited by the formation of this kind of strong filament. These filaments, known as surface negative sparks, were observed in previous work when the negative high voltage was higher than a threshold value [20–22].

The experiments reported here were carried out with a SDBD plasma actuator operating in a controlled atmosphere in order to investigate the contribution of nitrogen and oxygen ions to the ionic wind velocity and to the morphology of the plasma discharge. First, for each gas mixture, the consumed power was measured as a function of voltage amplitude. Then, for a given applied high voltage, the plasma morphology was recorded and lastly, ionic wind velocity measurements were performed. Results show that oxygen ions play the main role in ionic wind velocity production by a SDBD actuator. Nevertheless, the contribution of nitrogen to velocity is not negligible, especially on the acceleration length of the induced wall jet.

2. Experimental set-up

Experiments were conducted at atmospheric pressure in a 0.1 m^3 tank equipped with optical access for ICCD camera imaging (figure 1). A pressure probe of 1000 mbar in full range (Baratron MKS) was used to prepare different gas mixtures. The N_2/O_2 gas mixtures were kept at atmospheric pressure but the partial pressure of O_2 was gradually varied up to 100%. To change the mixture ratio, gases were evacuated by using a primary pump. Then the tank was filled with pure nitrogen ($[O_2] < 2$ ppmv and $[H_2O] < 3$ ppmv) to a pressure which was equal to the expected partial pressure for N_2 in mixture. Finally, pure oxygen ($[H_2O] < 3$ ppmv) was added until the total pressure in the tank reached the atmospheric pressure. As no secondary pump was used in this study, the concentration of residual gases in the gas mixtures was estimated to be less than 100 ppmv. As the velocity induced by the discharge is influenced by the relative humidity of the ambient air [12, 23, 24], artificial dry air mixed with dry gases (80% of N_2 and 20% of O_2) was chosen in preference to ambient air where the relative humidity cannot be precisely controlled. Note that the average measured velocity is around 10% lower in dry air than in ambient air in our experimental conditions [24].

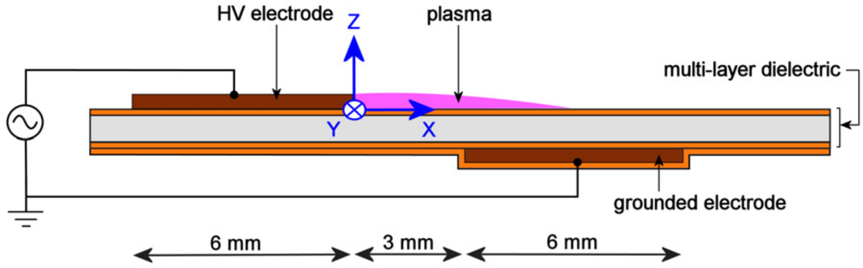

Figure 2. Sketch of the SDBD actuator.

As shown in figure 2, the SDBD consisted of two thin copper electrodes (80 μm thick in the Z-direction, 6 mm wide in the X-direction and 10 cm long in the Y-direction) mounted on both sides of a dielectric sheet 420 μm in thickness. The exposed electrode was connected to an ac power supply (Trek Amplifier 30/20A), the grounded one was placed below the dielectric sheet with a gap of 3 mm and encapsulated in order to produce discharges only on the upper side of the dielectric sheet. The dielectric was composed of Mylar covered on each side by one layer of polyimide film. The plasma was obtained by applying a sinusoidal high voltage to the exposed electrode.

As the behavior of a SDBD is a function of several parameters (i.e. high voltage amplitude and frequency, electrode shape, dielectric material and thickness, etc), the geometrical structure of this SDBD was optimized for plasma flow control applications, based on previous experimental studies [25–28]. Moreover, as this experimental work focused on the behavior of a SDBD plasma actuator in a controlled atmosphere, high-voltage amplitude and signal frequency remained unchanged ($V_{HV} = 12$ kV and $F_{HV} = 1$ kHz) during the study except for electrical power measurements (reported in section 3.1) where the voltage amplitude ranged from 4 to 15 kV. The induced low-velocity airflow was measured using a total pressure glass probe with a 0.5 mm entrance diameter section, moving along three axes X, Y and Z and connected to a pressure transducer (GE Druck LPM 9481 0.2 mbar) as illustrated in figure 1. The pressure transducer provides the differential pressure ΔP between the total pressure P_{tot} associated with the airflow and the static pressure P_{stat} measured in the tank, far from the induced flow. Airflow velocity was computed by using equation (1), where ρ is the gas mixture density calculated using the ideal gas law, expressed as a function of temperature and pressure.

$$\boldsymbol{U} = \sqrt{\frac{2 \cdot \Delta P}{\rho}}. \tag{1}$$

Experimental data correspond to a time-averaged value of the flow velocity. Voltage and current were measured with a high voltage probe and a current transformer probe. A 47 nF capacitor was used for power measurement. All electrical signals were recorded with a digital oscilloscope (Lecroy WaveSurfer 64Xs-A). Images of the discharge were acquired with an ICCD camera (Andor iStar DH734) equipped with a 60 mm focal lens (Nikon AF Micro Nikkor) with a typical gate width of 200 μs.

3. Experimental results and discussion

3.1. Electrical measurements

In figure 3(a), voltage and discharge current in dry air are plotted versus time with the sine applied high voltage. The discharge current is characterized by two distinct periods, corresponding to the discharges occurring during both cycles [24]. The positive-going cycle is characterized by high current pulses up to 250 mA (25 mA cm^{-1} for current per unit of the electrode length which was 10 cm) corresponding to streamer propagation. The negative-going half-cycle corresponds to a glow regime, characterized by small current pulses up to several tens of mA.

Voltage and current are plotted versus time for one ac cycle in pure nitrogen (figure 3(b)) and pure oxygen (figure 3(c)). In pure nitrogen, current pulses were smaller than in dry air during the positive-going cycle. However, this cycle started earlier, when the high voltage was still negative. This was due to the presence of residual charges from the former cycle. As this discharge cycle was longer than in dry air, the number of current pulses was higher. In pure oxygen, the number of current pulses was smaller than in dry air and pure nitrogen during the positive half-cycle but their intensity was higher up to 400 mA. Moreover, in pure oxygen, strong negative pulses can be observed during the negative-going cycle which underlined the propagation of negative spark filaments (section 3.2).

In order to compare the electrical characteristics of the plasma actuator in various gases, the electrical power was measured since it can be a key parameter to assess the actuator efficiency as reported in [29]. A common method, consisting in using a capacitor in series with the actuator and in calculating the $Q - V_{HV}$ cycle area [30, 31], was used to estimate the power consumption (2). Experimental data curves were fitted by a power law function (3) according to our experimental configuration [25], where V_0 and A are constants based on geometry, dielectric thickness and gas composition. From this formula, one can notice that the power is equal to zero for $V_{HV} = V_0$; consequently, this value is often considered as the threshold value of plasma ignition [25].

$$\boldsymbol{P}_{elec} = F_{HV} \int_{cycle} V_{HV} \cdot dQ \tag{2}$$

$$\boldsymbol{P}_{elec} \propto A \cdot F_{HV} (V_{HV} - V_0)^2. \tag{3}$$

Results are presented in figure 4 for three different gas mixtures: artificial dry air, pure nitrogen and pure oxygen.

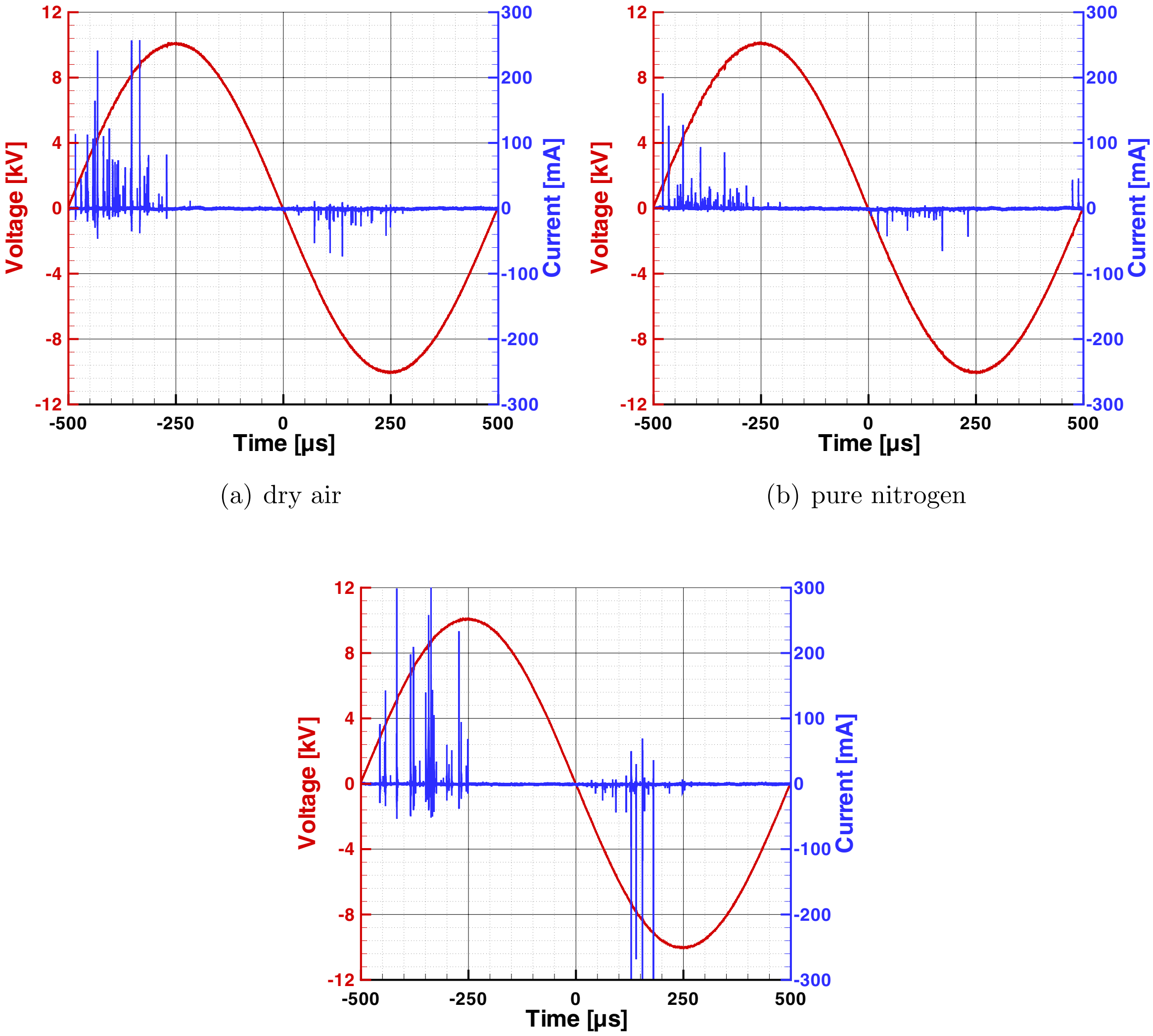

(a) dry air

(b) pure nitrogen

(c) pure oxygen

Figure 3. Voltage and current versus time for one ac cycle in dry air (*a*), pure nitrogen (*b*) and pure oxygen (*c*). $V_{HV} = 10$ kV and $F_{HV} = 1$ kHz.

The electrical power consumption is plotted against the high voltage amplitude with a constant frequency of $F_{HV} = 1$ kHz. It can be seen that the power consumption differs when the gas changes at a given voltage. For instance, at $V_{HV} = 12$ kV, the electrical power consumption was around 75 W m^{-1} in pure oxygen, 80 W m^{-1} in dry air and 95 W m^{-1} in pure nitrogen. For a voltage lower than 14 kV, the power consumption was the highest in pure nitrogen and the lowest in pure oxygen.

The threshold values of the plasma ignition for the three gases are given in table 1. This value was the smallest in pure nitrogen and the highest in pure oxygen and corresponds to an electrical field necessary for the electrical breakdown (i.e. breakdown voltage) of a gas of a given composition. Generally, it is admitted that a gas discharge at high pressure takes place when the ionization rate exceeds the rate of electron attachment. The electrical field where these two rates are equally balanced is called the critical field. The ionization energy of O_2 is a little smaller than that of N_2, but as O_2 is an electronegative gas, the critical field for a N_2/O_2 gas mixture increases with the proportion of O2 [32]. Indeed, according to the calculation of Dubois *et al* [32] for a N_2/O_2 gas mixture kept at atmospheric pressure, the reduced critical electrical field increments from 75 to 126.6 Td when the proportion of O_2 increases from 0 to 100%. According to their experimental investigation of corona discharge in air and N_2/O_2 mixtures, the increase in the O_2 concentration leads to a drop in the average current due to a rise of electron attachment. This can explain why the addition of oxygen atoms in pure nitrogen induced a reduction in the electrical power consumption and a delay in the plasma discharge ignition. However, this difference decreased when the voltage rose. At 13.5 kV, the power consumption was equivalent in dry air and in pure oxygen, around 130 W m^{-1}. Previous measurements showed that in dry air, when the voltage was high enough, negative spark filaments started propagating during the negative half-cycle indicating the transition from a diffuse to a filamentary regime [24]. According to the experimental data shown in figure 4, the consumed power increased faster in pure oxygen when the applied voltage was higher than 13 kV. As the latter voltage corresponded to the occurrence of negative spark filaments

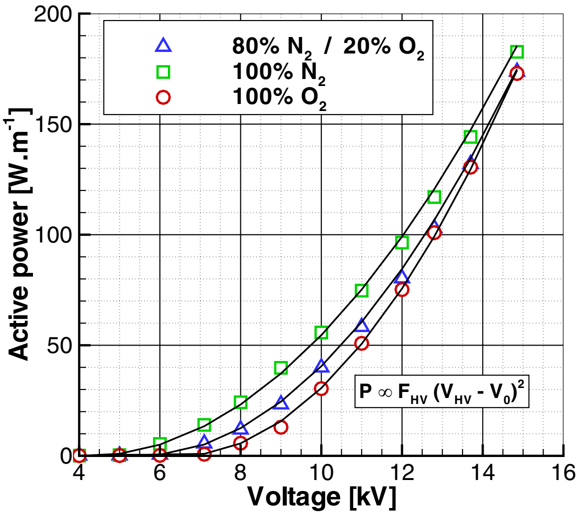

Figure 4. Electrical power per unit of electrode length against the high voltage amplitude for three N_2/O_2 ratios, $F_{HV} = 1$ kHz.

Table 1. Power law parameters versus gas mixture.

Gas mixture	V_0 (kV)	A ($W\,m^{-1}\,Hz^{-1}\,kV^{-2}$)
Air (80/20 vol ratio)	5.5	2×10^{-3}
Pure nitrogen	4.25	1.65×10^{-3}
Pure oxygen	6.5	2.5×10^{-3}

(section 3.2) characterized by strong negative current pulses (figure 3(*c*)), it can be deduced that negative spark filaments were responsible for the increase in the consumed power observed at a high O_2 level.

3.2. Plasma morphology

As already mentioned, all the experiments below were performed with the same electrical parameters (i.e. $V_{HV} = 12$ kV and $F_{HV} = 1$ kHz). Figure 5 shows pictures of a plasma discharge created in different gas mixtures. The evolution of the plasma, from pure nitrogen (top) to pure oxygen (bottom), is illustrated in negative gray-scale for both half-cycles. Images were recorded with a gate width of 200 μs which is about a quarter-cycle. Note that the direction of the ionic wind goes from the HV electrode to the grounded one.

Positive half-cycle: in pure nitrogen, plasma filaments spread over the dielectric until the end of the grounded electrode. The discharge distribution seems quasi-homogeneous even if the light intensity was slightly higher close to the HV electrode. When the volumetric ratio of oxygen increased, the length and number of filaments decreased and the discharge became less homogeneous. Up to a global volumetric ratio of 50/50, global light intensity decreased. On increasing the oxygen ratio further, the light intensity increased over the gap. In pure oxygen, the discharge was no longer homogeneous. The number of channels decreased and they became much broader. These filaments were shorter and only extended to the edge of the grounded electrode ($x = 3$ mm) where they appeared much stronger. Pancheshnyi *et al* [33] observed, in the case of a point-to-plane discharge, that adding a few percent of O_2 in pure nitrogen led to a decrease of 40% in the intensity of the electrical field at the head of a streamer. This can explain why the length of the discharge appeared shorter on the ICCD pictures, for the positive half-cycle, when the proportion of O_2 increased. Furthermore, many plasma filaments seemed to ignite at the same location and follow the same channels along the gap, also resulting in an increase in light intensity. This is a good correlation with the fact that the current pulses in pure oxygen were the highest and the fewest in comparison with those in dry air or in pure nitrogen.

Negative half-cycle: in pure nitrogen, the filaments were shorter and the light intensity lower than in the positive half-cycle. Filaments were more diffuse and their length did not exceed 5 mm. When the volumetric ratio of oxygen increased, filaments became longer. Up to a global volumetric ratio of 70/30, some of these strong ionized channels went straight over the gap and branched when they reached the middle of the grounded electrode ($x = 6$ mm). These negative sparks have also been observed in ambient air [19–22]. As the concentration of O_2 increased, the volumetric charge increased and if this concentration became high enough, negative spark breakdowns occurred [18]. This underlines that the propagation of such filaments was linked to the proportion of O_2 in the gas mixture. More precisely, the threshold value of the negative spark breakdowns decreased when the proportion of O_2 increased. In pure oxygen, the propagation of one of these filaments corresponded to a strong negative current peak (section 3.1). These strong channels dominated the discharge and ignited at almost the same location. This can be explained by the charge distribution on the dielectric surface, due to a former discharge activity. Note that in pure nitrogen, a weak glow discharge was observed without any waves of near surface luminosity. However, the properties of the actuator, the electrical parameters and especially the ICCD gate width of our experiment were different from those of Leonov *et al* [13]. This can explain why the pictures of these two studies are different.

3.3. Induced ionic wind velocity measurements

The first series of measurements concerned the characterization of velocity profiles along the Y-direction indicated in figure 2. Velocity is plotted in figure 6(*a*) as a function of Y for artificial dry air (80% of N_2 and 20% of O_2). Note that $x = 6$ mm corresponds to the middle of the grounded electrode in the stream-wise direction and $z = 0.25$ mm is the lowest position which can be measured in this study. Note that even if this tube position may influence the discharge, this low z-value was chosen because close to the high voltage electrode, the maximum velocity value was located close to the dielectric surface (figure 6(*b*)). The velocity fluctuated quasi-periodically along the span-wise direction. One might think that this periodicity is due to regular roughness at the edge of the copper high voltage electrode, since the electric field is enhanced periodically in this case and the momentum transfer increases [34]. But a careful examination showed that there was no roughness periodicity. The periodicity is more likely due to a quasi-regular distribution of the streamer along the electrode. A more detailed study is necessary to understand

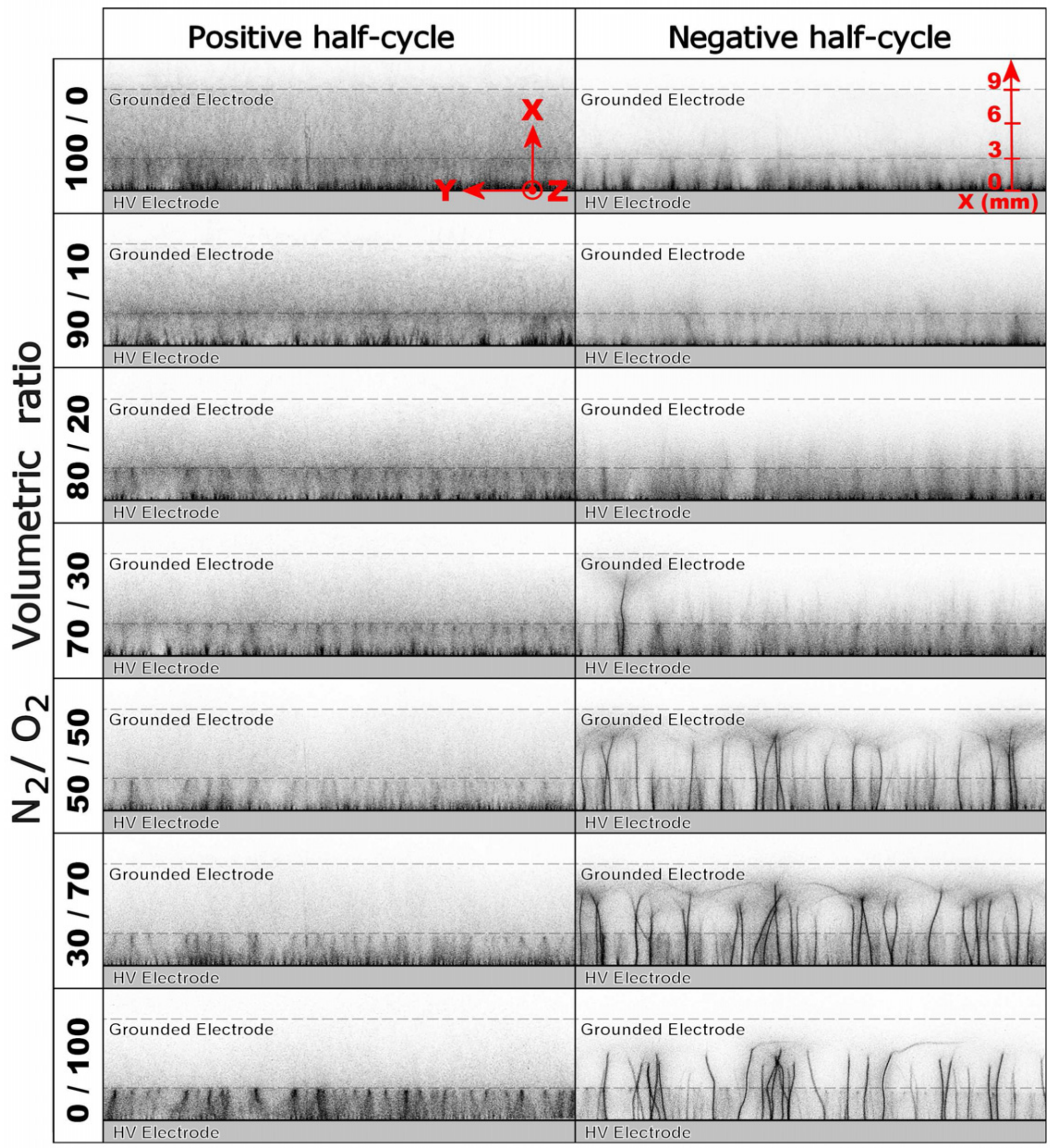

Figure 5. Plasma morphology for both half-cycles as a function of the N_2/O_2 volumetric ratio. $V_{HV} = 12$ kV and $F_{HV} = 1$ kHz. Gate width of 200 μs with a delay of 100 μs after the beginning of each half cycle.

this observation. For all the following measurements, the position along the Y-direction was set at $y = 2$ mm where the maximum ionic wind velocity was observed.

The second series of measurements concerned the characterization of velocity profiles along the X-direction indicated in figure 2. Velocity evolution is plotted in figure 6(*b*) as a function of X for three different gas mixtures: artificial dry air (80% of N_2 and 20% of O_2), pure nitrogen and pure oxygen. For these three gases, the velocity increased from the edge of the upper electrode, reached a maximum and then decreased. It can be seen that the maximum for dry air was the highest while that of pure nitrogen was the lowest. The velocity in pure oxygen was higher than that in pure nitrogen (about twice), but lower than in dry air (15% less). Otherwise, the velocity reached its maximum more quickly in pure oxygen than in dry air or in pure nitrogen where the ionic wind diffusion area is longer (the positions of the velocity maxima are 3.5 mm, 6 mm and 7.5 mm respectively). This indicates that a stronger ionic wind is induced in oxygen than in nitrogen, even if the ionic wind produced in nitrogen is not negligible. As the ionic wind velocity is influenced by the size of the grounded electrode, its size was chosen to maximize the velocity in ambient air [2, 25] and not in pure nitrogen. A longer grounded electrode might induce a higher ionic wind velocity in pure nitrogen.

The third series of measurements concerned the characterization of velocity profiles along the Z-direction. Velocity evolution is plotted in figure 7 as a function of Z for three X-values corresponding to the beginning, the middle and the end of the grounded electrode. In pure nitrogen, the induced velocity was always about 70% lower than in the other mixtures. In pure oxygen, the induced velocity was twice as high as in dry air over the gap ($x = 0$ mm to $x = 3$ mm) but dropped to about 20% lower just after the beginning of the grounded electrode. Furthermore, whatever

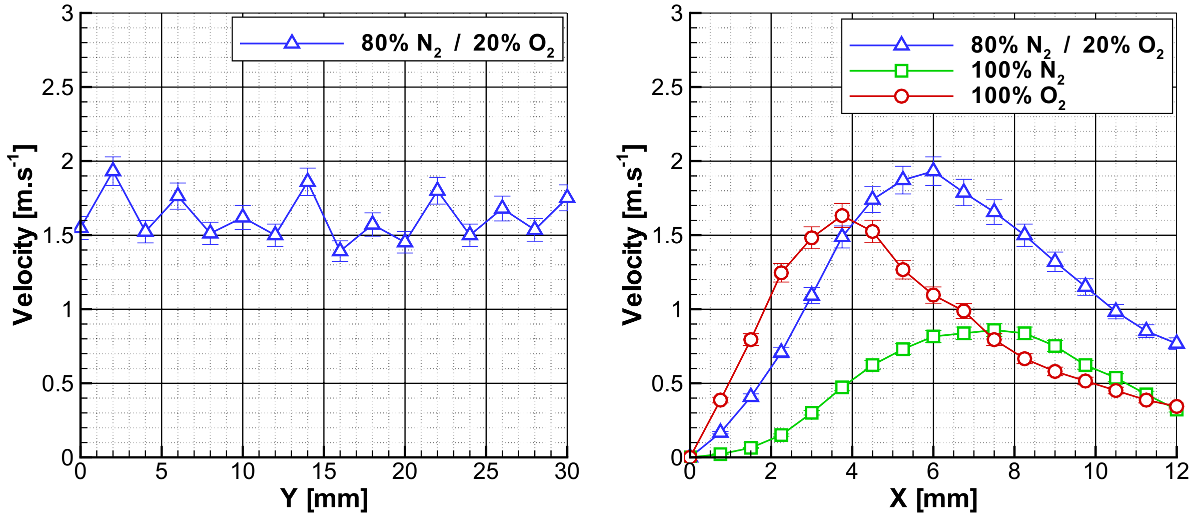

(a) x=6 mm and z=0.25 mm (b) y=2 mm and z=0.25 mm

Figure 6. Ionic wind velocity along the Y-direction (a) and along the X-direction (b). $V_{HV} = 12$ kV and $F_{HV} = 1$ kHz.

the mixture, the Z-position of the maximum velocity increased as X increased which is indicative of a wall-jet induced flow behavior with an acceleration zone (figure 7(a)) and a diffusion zone (figure 7(c)). As the plasma extension was longer in pure nitrogen than in dry air, the acceleration length of the induced wall jet was larger. These results show that the induced velocity in air is mostly due to the contribution of oxygen ions, as discussed in previous work [13, 17]. However, the contribution of nitrogen ions is not negligible, especially over the end of the grounded electrode. Indeed, the location of the maximum ionic wind velocity in pure nitrogen (figure 8(b) with triangle symbols) corresponded to the end of the plasma extension during the positive half-cycle (figure 5). This can be explained by the fact that during the positive half-cycle, plasma filaments spread over the dielectric until the end of the grounded electrode and a positive surface charge was then created at this location, leading to momentum transfer during the relaxation phase between two micro-discharges [13]. As the number of micro-discharges was high in pure nitrogen (i.e. high number of current peaks), the contribution of nitrogen ions was not negligible in ionic wind velocity production.

Finally, the ionic wind velocity along the X-direction is plotted in figure 8(a) for several N_2/O_2 volumetric ratios. In figure 8(b), the maximum velocity value and its location are plotted as a function of the percentage of O_2 in the gas (mixed with N_2, the total pressure is always 1 atm). The location of the maximum velocity shifted away from the high voltage electrode as the ratio of O_2 in gas decreased (figure 8(b) with triangle symbols). By replacing 10% of pure nitrogen with oxygen, the velocity doubled, but a further addition of oxygen led to a decrease in the velocity (figure 8(b) with circle symbols). More precisely, when the percentage of O_2 in dry air dropped from 20% to 10%, the ionic wind velocity increased very slightly but the lack of oxygen in dry air induced a significant drop in this velocity which is reduced by half by suppressing the last 10% of oxygen. This underlines the important role played by oxygen ions in ionic wind velocity production.

The maximum velocity measured in dry air for $z = 0.25$ mm was around 1.9 m s^{-1}; an increase in O_2 from 20% to 30% in the gas mixture was responsible for a 10% decrease in this value. ICCD measurements showed that the propagation of negative spark filaments was linked to the proportion of O_2 (section 3.2). More precisely, they underlined that the increase in O_2 from 20% to 30% in the gas mixture was also responsible for the propagation of negative spark filaments during the negative half-cycle. This confirms that the maximum induced velocity was limited by the propagation of such filaments. By increasing again the concentration of O_2 in the gas mixture, the maximum velocity value kept decreasing slowly and then became constant when this concentration exceeded 70%. From this observation, it can be concluded that when the concentration of O_2 in the gas mixture increased, for constant electrical parameters (i.e. $V_{HV} = 12$ kV and $F_{HV} = 1$ kHz), the saturation effect shifted to lower voltages, which limited the maximum ionic wind velocity to lower values. To explain this result and the propagation of negative spark filaments, results from a numerical simulation have been used [18].

During the negative half-cycle, glow discharges seed the dielectric region with negative oxygen ions and electrons which form a negative volumetric charge leading to momentum transfer [18]. By increasing the high voltage amplitude, the length of the filaments increases and their structure becomes less diffuse and more luminous (figure 5). The negative volumetric charge also increases, resulting in a gain of momentum transfer. If the volumetric charge becomes high enough to screen the electric field, spark breakdowns occur and the gain of momentum transfer cannot increase any more [18]. When the concentration of O_2 in the gas mixture increases, for constant electrical parameters, the negative volumetric charge also increases and the threshold value to screen the electric field (i.e. for negative spark filaments to propagate) becomes smaller. Therefore the saturation effect is shifted to

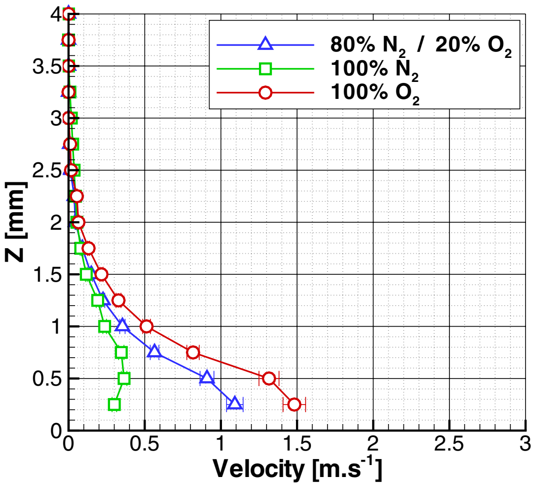

(a) y=2 mm and x=3 mm

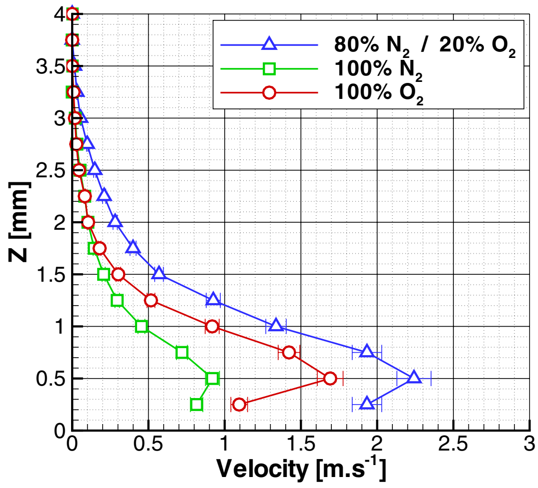

(b) y=2 mm and x=6 mm

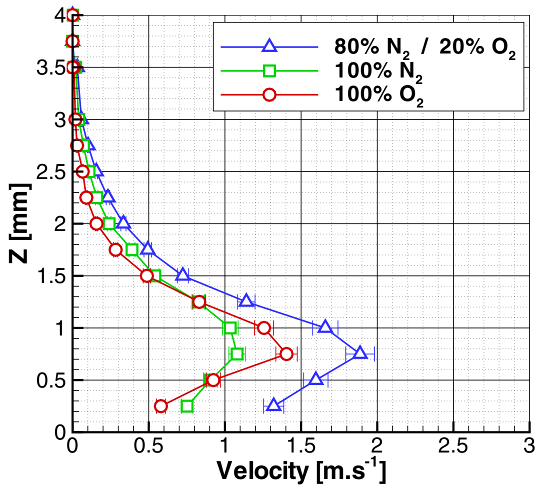

(c) y=2 mm and x=9 mm

Figure 7. Ionic wind velocity U_X along the Z-direction for three N_2/O_2 ratios. $V_{HV} = 12$ kV and $F_{HV} = 1$ kHz.

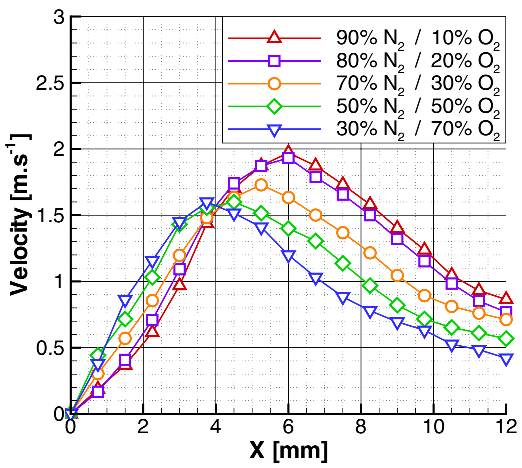

(a) y=2 mm and z=0.25 mm

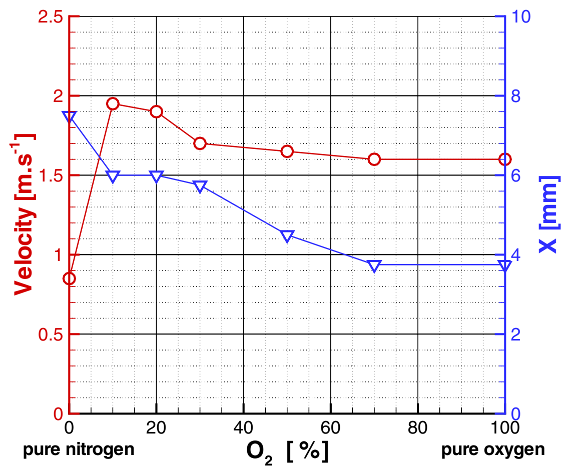

(b) y=2 mm and z=0.25 mm

Figure 8. Ionic wind velocity U_X along the X-direction for different N_2/O_2 ratios (a). Evolution of the maximum ionic wind velocity (circle symbols) and its location (triangle symbols) for different percentages of O_2 in air (b). $V_{HV} = 12$ kV and $F_{HV} = 1$ kHz.

lower voltages and the maximum ionic wind velocity value decreases. These experimental results are in good agreement with the hypothesis that the momentum transfer induced by a SDBD plasma actuator is mainly due to oxygen negative ion accumulation inside a volume above the dielectric [18].

4. Conclusion

This paper has presented an experimental investigation of a surface DBD Plasma Actuator operating in a controlled atmosphere. Electrical power consumption, ICCD imaging and mean velocity measurements were done with regard to the N_2/O_2 volumetric ratio. Experimental measurements revealed some features of the contribution of nitrogen and oxygen ions to the ionic wind velocity and to the morphology of the plasma discharge.

- For a given frequency of high voltage, the power consumption is influenced by the N_2/O_2 volumetric ratio. The electrical power consumed is greater when the discharge is in pure nitrogen where the plasma extension is longer and the number of filaments is higher than in pure oxygen. Moreover plasma ignition occurs later in oxygen due to the higher electron attachment property of oxygen.
- The morphology of the plasma filaments is also influenced by the N_2/O_2 volumetric ratio. During the positive half-cycle, the length of the filaments and their number decrease as the concentration of O_2 increases. During the negative half-cycle, negative sparks appear when the concentration of O_2 increases.
- The important role played by oxygen ions in momentum transfer was confirmed. Induced ionic wind velocity is mainly due to oxygen negative ions during the negative half-cycle. Nevertheless, the contribution of nitrogen to velocity is not negligible during the positive half-cycle.
- The maximum induced velocity is limited by the propagation of negative spark filaments during the negative half-cycle. The propagation of such filaments is linked to the proportion of O_2 in the gas mixture. Increasing this proportion leads to a shift in the saturation effect to lower voltages and to a decrease of the maximum ionic wind velocity value.

The results presented here have underlined the influence of nitrogen and oxygen on the behavior of a SDBD actuator and are expected to supply information for future experimental investigations and numerical simulations to improve the potential of such actuators for flow control. As electrical parameters were kept constant during this study, no conclusive correlation was obtained between plasma extension and location of the maximum velocity. Phase-averaged velocity measurements need to be performed, in correlation with ICCD imaging, in nitrogen and oxygen to further analyze the mechanisms of induced momentum transfer. Furthermore, computation of the mass flow rate from phase-averaged measurements will lead to an estimation of the DBD efficiency with regard to the N_2/O_2 volumetric ratio.

References

[1] Corke T C, Enloe C L and Wilkinson S P 2010 Dielectric barrier discharge plasma actuators for flow control *Annu. Rev. Fluid Mech.* **42** 505–29

[2] Bénard N and Moreau E 2012 EHD force and electric wind produced by surface dielectric barrier discharge plasma actuators used for airflow control *6th AIAA Flow Control Conf.* vol 3136 (AIAA)

[3] Wang J-J, Choi K-S, Feng L-H, Jukes T N and Whalley R D 2013 Recent developments in DBD plasma flow control *Prog. Aerospace Sci.* **62** 52–78

[4] Bénard N, Moreau E, Griffin J and Cattafesta L N 2010 Slope seeking for autonomous lift improvement by plasma surface discharge *Exp. Fluids* **48** 791–808

[5] Little J, Nishihara M, Adamovich I and Samimy M 2010 High-lift airfoil trailing edge separation control using a single dielectric barrier discharge plasma actuator *Exp. Fluids* **48** 521–37

[6] Grundmann S and Tropea C 2009 Experimental damping of boundary-layer oscillations using DBD plasma actuators *Int. J. Heat Fluid Flow* **30** 394–402

[7] Joussot R, Hong D, Weber-Rozenbaum R and Leroy-Chesneau A 2010 Modification of the laminar-to-turbulent transition on a flat plate using a DBD plasma actuator *5th AIAA Flow Control Conf.* vol 4708 (AIAA)

[8] Lagmich Y, Callegari Th, Pitchford L C and Boeuf J P 2008 Model description of surface dielectric barrier discharges for flow control *J. Phys. D: Appl. Phys.* **41** 095205

[9] Boeuf J P, Lagmich Y and Pitchford L C 2009 Contribution of positive and negative ions to the electrohydrodynamic force in a dielectric barrier discharge plasma actuator operating in air *J. Appl. Phys.* **106** 023115

[10] Bénard N, Balcon N and Moreau E 2008 Electric wind produced by a surface dielectric barrier discharge operating in air at different pressures: aeronautical control insights *J. Phys. D: Appl. Phys.* **41** 042002

[11] Versailles P, Gingras-Gosselin V and Vo H D 2010 Impact of pressure and temperature on the performance of plasma actuators *AIAA J.* **48** 859–63

[12] Anderson R and Roy S 2006 Preliminary experiments of barrier discharge plasma actuators using dry and humid air *44th AIAA Aerospace Sciences Meeting and Exhibit (9–12 Jan 2006, Reno, Nevada)* vol 0369 (AIAA)

[13] Leonov S, Opaits D, Miles R and Soloviev V 2010 Time-resolved measurements of plasma-induced momentum in air and nitrogen under dielectric barrier discharge actuation *Phys. Plasmas* **17** 113505

[14] Bénard N, Pons J, Audier P, Moreau E, Hong D and Leroy-Chesneau A 2011 Filaments in a surface dielectric barrier discharge operating in altitude conditions *IEEE Trans. Plasma Sci.* **39** 2222–23

[15] Forte M, Jolibois J, Pons J, Moreau E, Touchard G and Cazalens M 2007 Optimization of a dielectric barrier discharge actuator by stationary, non-stationary measurements of the induced flow velocity: application to airflow control *Exp. Fluids* **43** 917–28

[16] Kim W, Do H, Mungal M G and Cappelli M A 2007 On the role of oxygen in dielectric barrier discharge actuation of aerodynamic flows *Appl. Phys. Lett.* **91** 181501

[17] Enloe C L, McHarg M G and McLaughlin T E 2008 Time-correlated force production measurements of the dielectric barrier discharge plasma aerodynamic actuator *J. Appl. Phys.* **103** 073302

[18] Soloviev V R 2012 Analytical estimation of the thrust generated by a surface dielectric barrier discharge *J. Phys. D: Appl. Phys.* **45** 025205

[19] Thomas F, Corke T, Iqbal M, Kozlov A and Schatzman D 2009 Optimization of dielectric barrier discharge plasma actuators for active aerodynamic flow control *AIAA J.* **47** 2169–78

[20] Larigaldie S 1987 Spark propagation mechanisms in ambient air at the surface of a charged dielectric. experimental: the main stages of the discharge *J. Appl. Phys.* **61** 90

[21] Merrill F H and Von Hippel A 1939 The atomphysical interpretation of Lichtenberg figures and their application to the study of gas discharge phenomena *J. Appl. Phys.* **10** 873–87

[22] Joussot R, Boucinha V, Weber R and Hong D 2011 Negative spark leaders on a surface DBD plasma actuator *Plasma Science, IEEE Transactions on* **39** 2194–5

[23] Benard N, Balcon N and Moreau E 2009 Electric wind produced by a surface dielectric barrier discharge operating over a wide range of relative humidity *47th AIAA Aerospace Sciences Meeting* vol 488 (AIAA)

[24] Audier P, Rabat H, Hong D and Leroy A 2012 Influence of the N_2/O_2 volumetric ratio on the behavior of a SDBD plasma actuator *6th Flow Control Conf. (New Orleans, LA)* vol 3094 (AIAA)

[25] Boucinha V, Magnier P, Leroy-Chesneau A, Weber R, Joussot R, Dong B and Hong D 2008 Characterization of the ionic wind induced by a sine DBD actuator used for laminar-to-turbulent transition delay *4th Flow Control Conf. (Seattle, Washington, DC)* vol 4210 (AIAA)

[26] Magnier P, Boucinha V, Dong R, Weber B, Leroy-Chesneau A, Hong D and Hureau J 2009 Experimental study of the flow induced by a sinusoidal dielectric barrier discharge actuator and its effects on a flat plate natural boundary layer *J. Fluids Eng.* **131** 011203

[27] Audier P, Leroy A and Hong D 2012 Unsteady forcing of a post-stall flow over a NACA 0012 airfoil by a surface DBD actuator. *6th Flow Control Conf. (New Orleans, LA)* vol 3052 (AIAA)

[28] Joussot R, Weber R, Leroy A and Hong D 2013 Transition control using a single plasma actuator *Int. J. Aerodyn.* **3** 26–46

[29] Kriegseis J, Grundmann S and Tropea C 2011 Power consumption, discharge capacitance and light emission as measures for thrust production of dielectric barrier discharge plasma actuators *J. Appl. Phys.* **110** 013305

[30] Enloe C L, McLaughlin T E, Van Dyken R D, Kachner K D, Jumper E J and Corke T C 2004 Mechanisms and responses of a single dielectric barrier plasma actuator: plasma morphology *AIAA J.* **42** 589–94

[31] Pons J, Moreau E and Touchard G 2005 Asymmetric surface dielectric barrier discharge in air at atmospheric pressure: electrical properties and induced airflow characteristics *J. Phys. D: Appl. Phys.* **38** 3635

[32] Dubois D, Merbahi N, Eichwald O, Yousfi M and Benhenni M 2007 Electrical analysis of corona discharge in air, N_2, O_2 and CO_2 mixtures *J. Appl. Phys.* **101** 053304

[33] Pancheshnyi S V, Starikovskaia S M and Starikovskii A Yu 2001 Role of photoionization processes in propagation of cathode-directed streamer *J. Phys. D: Appl. Phys.* **34** 105

[34] Leonov S, Opaits D, Miles R and Soloviev V 2010 Time-resolved measurements of plasma-induced momentum in air and nitrogen under dielectric barrier discharge actuation *Phys. Plasmas* **17** 113505